Towards Industrial-Strength Navier-Stokes Codes

Wen-Huei Jou, Laurence B. Wigton, Steven R. Allmaras,
Philippe R. Spalart, N. Jong Yu

Boeing Commercial Airplane Group
P.O. Box 3707, MS 7H-96
Seattle, WA 98124-2207

Abstract

In this paper we discuss our experiences with Navier-Stokes (NS) codes using central differencing (CD) and scalar artificial dissipation (SAD). NS-CDSAD codes have been developed by Jameson, Martinelli, Swanson, and Vatsa among others. Our results confirm that for typical commercial transport wing and wing/body configurations flying at transonic conditions with all turbulent boundary layers, NS-CDSAD codes, when used with the Johnson-King turbulence model, are capable of computing pressure distributions in excellent agreement with experimental data. However, results are not as good when laminar boundary layers are present. Exhaustive 2–D grid refinement studies supported by detailed analysis suggest that the numerical errors associated with SAD severely contaminate the solution in the laminar portion of the boundary layer. It is left as a challenge to the CFD community to find and fix the problems with Navier-Stokes codes and to produce a NS code which converges reliably and properly captures the laminar portion of the boundary layer on a reasonable grid.

Introduction

Boeing's recent acquisition of a CRAY Y-MP has enabled us to perform definitive grid-refinement studies with NS codes. We will focus attention on Jameson-technology (JT) codes developed by, among others, Jameson [1], Martinelli [2], Swanson [3], and Vatsa [4]. JT-NS codes employ central differences (CD) with scalar artificial dissipation (SAD). From the point of view of accuracy in a Navier-Stokes calculation, CDSAD is thought by some not to be as good as other available methods. Indeed, van Leer [5] boldly states that there is no hope for the flux formula of the Jameson type. Nonetheless, the combination of CDSAD with Runge-Kutta time marching, augmented with implicit residual smoothing and multigrid, have given JT codes a well deserved reputation of being fast and reliable compared to other available methodologies. Thus JT-NS codes have achieved a wide following in the CFD community.

In this paper we will present some applications of JT-NS codes to 3–D and 2–D problems of aerodynamic interest, including wing/body, nacelle, airfoil and multi-element airfoil configurations.

We will begin our discussion with an account of the relative success of JT-NS codes applied to 3–D wing/body configurations with turbulent flow. We will follow with a somewhat sadder tale for 2–D airfoils involving runs of laminar flow. Our attempts to locate the problems with 2–D JT-NS have included detailed grid refinement studies which indicate numerical problems particularly in the laminar portion of the boundary layer. These numerical problems are discussed at length. The inability of JT-NS codes to properly capture the laminar portion of the boundary layer (on a reasonable grid) prevents us from including a stability analysis needed to predict the onset of transition. We give examples where transition prediction is very important, including flow around a high-lift multi-element airfoil configuration and for around a nacelle.

Wing and Wing/Body Analysis and Design

In this section we will compare the capabilities of the JT-NS code TLNS3D developed at NASA Langley [4], using the Johnson-King turbulence model [6] , with our traditional viscous/inviscid coupled code A488.

In figure (1) we show a comparison, for a supercritical wing near design conditions, between experimental data, TLNS3D, and A488. The TLNS3D solution matches well with test data, whereas the A488 solution places the shock too far back. For the many test cases, TLNS3D has proven to be consistently more accurate than A488 [7, 8].

Another advantage TLNS3D enjoys over A488 is the ability to predict flows at off-design conditions involving

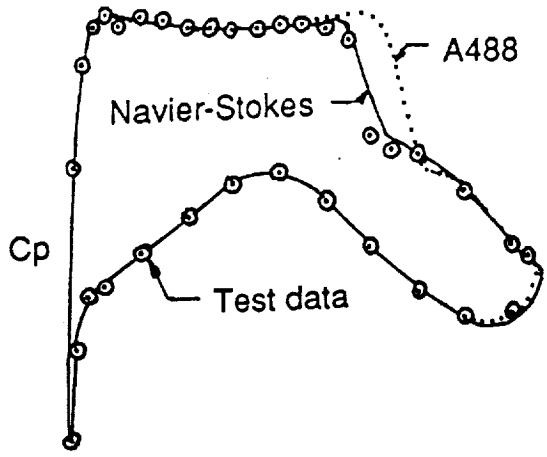

Figure 1: 3–D Navier-Stokes versus A488

flow separation. Figure (2) shows wing upper surface streamlines and pressure distributions at 65% semispan station. TLNS3D properly predicts the trailing edge separation and detailed surface pressures.

Encouraged by these successful analysis runs using TLNS3D, work has begun on design. An iterative design method that allows the designer to prescribe desired pressure distributions together with geometry constraints, such as thickness and trailing edge closure is under development. Preliminary results based on this method are shown in figure (3). Here the target geometry is the ONERA M6 wing, and the pressure distributions are given. Beginning with a NACA 0012 wing section as an input geometry, the target geometry is accurately recovered within 20 design cycles. A more detailed description of the design method is under preparation [9].

Practical CFD Assessment for Wing/Body

Generally speaking, the ability of TLNS3D to properly predict the pressures at both cruise and slightly off-design conditions is good. The main problems are laminar flow predictions and accurate drag predictions. Accurate drag predictions are crucial to design/optimization. Indeed, one of the design goals is to maximize the lift-to-drag ratio (under constraints). The designer will make a considerable effort to reduce drag by even as little as 1%. It is estimated that a 1% drag reduction, for a long-range airplane such as the Boeing 777, will save the airlines 6 billion dollars, based on a 2,000 airplane fleet operating over a 20 year service life [10]. Customer airlines require that tight performance guarantees be offered years before the airplane is actually built. In this tough commercial environment, the accuracy and reliability requirements must be very high if CFD is to be depended on to help fine tune final

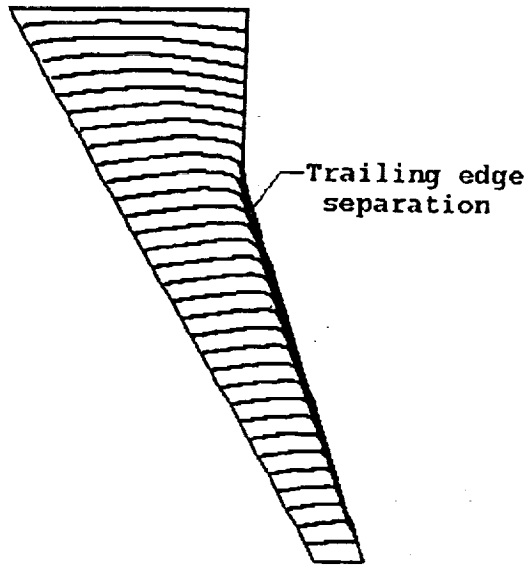

a. Upper surface streamlines

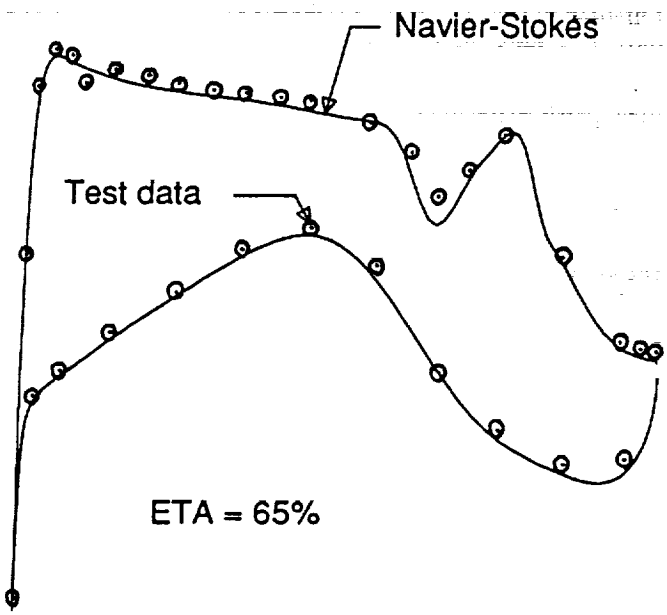

b. Pressure distributions

Figure 2: 3–D Navier-Stokes Streamlines and Pressures at 65% semispan

INVERSE DESIGN WITH NAVIER STOKES

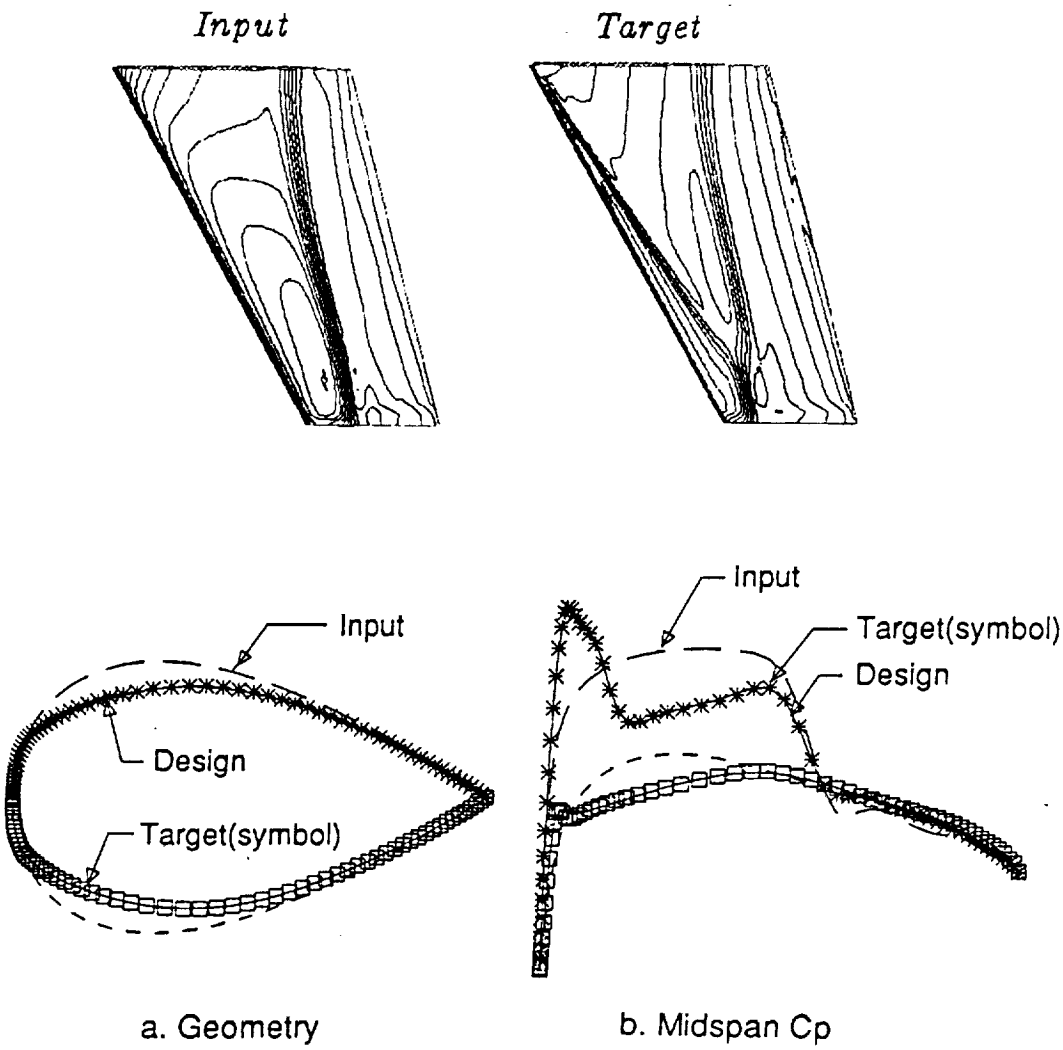

Figure 3: 3-D Navier-Stokes Design

designs and to establish meaningful performance guarantees.

2–D Airfoil Studies

The most direct 2–D equivalent to TLNS3D is the JT-NS code FLOMGE developed by Swanson [3] which also incorporates the Johnson-King turbulence model. For some flow situations, FLOMGE gives reasonable results. An example involving RAE 2822 case 6 is shown in figure (4).

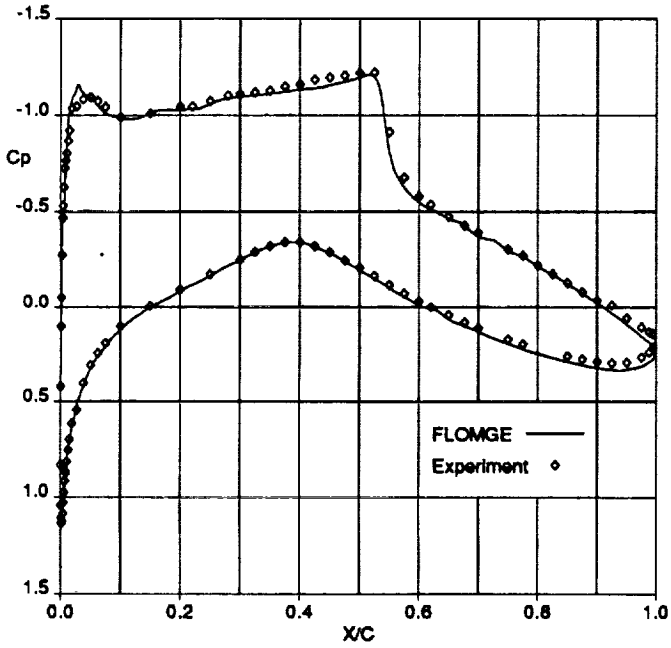

Figure 4: RAE 2822 Case 6 Surface Pressures; Comparison of FLOMGE with Johnson-King Model and Experiment [15]

There are, however, data cases which stress the credibility of all currently available 2–D airfoil codes. An apparently innocuous example is provided by the NACA 0012 airfoil at zero incidence. This condition removes the angle of attack as a "Fudge Factor". In figures (5) and (6) we compare experimental data [15] with results computed by FLOMGE and ISES (viscous/inviscid coupled code developed by Giles and Drela [13]) at two different Mach numbers. The solutions computed by FLOMGE and ISES agree well with each other at the lower Mach number, but the computed shock locations are too far back on the airfoil. At the higher Mach number, the ISES result is a little better than the FLOMGE solution, but again the shocks are too far back. The transition point for these calculations was placed at 3% of chord, but changing the transition point location drastically, say to 40% of chord, changes the shock location very little. These poor test/theory comparisons are present not only for ISES and FLOMGE but for all

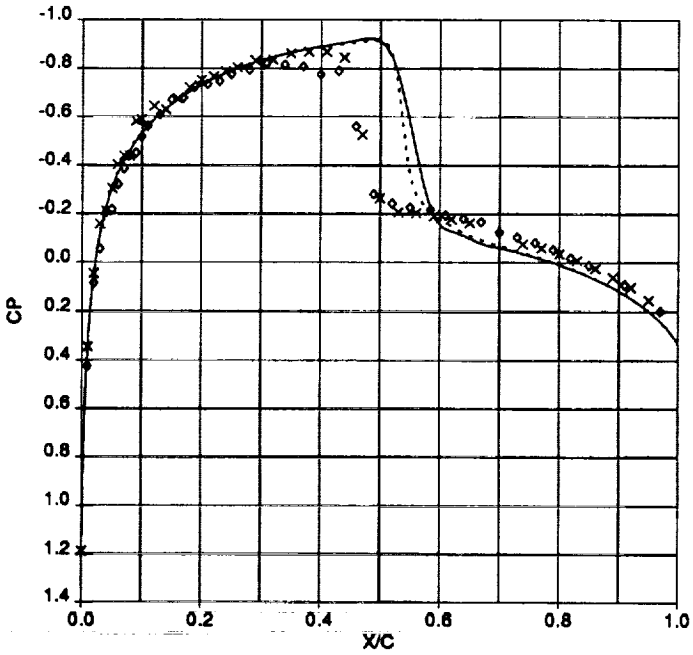

Figure 5: NACA 0012, experiment (Symbols) versus FLOMGE (Solid Line) and ISES (Dashed Line) at $M = 0.814$, $Re = 24.7 \times 10^6$, $\alpha = 0°$

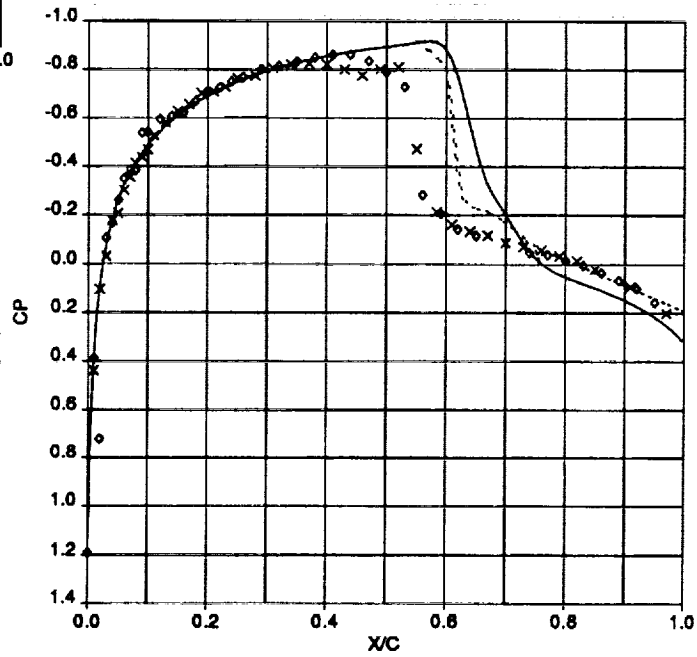

Figure 6: NACA 0012, experiment (Symbols) versus FLOMGE (Solid Line) and ISES (Dashed Line) at $M = 0.835$, $Re = 24.7 \times 10^6$, $\alpha = 0°$

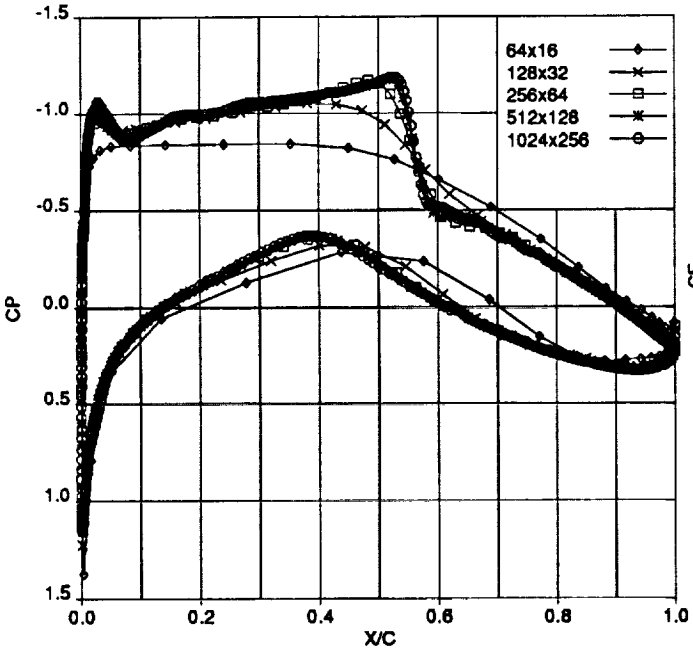

Figure 7: Pressure Distributions Computed on a Sequence of Grids (64×16) through (1024×256) for RAE 2822 Case 7.

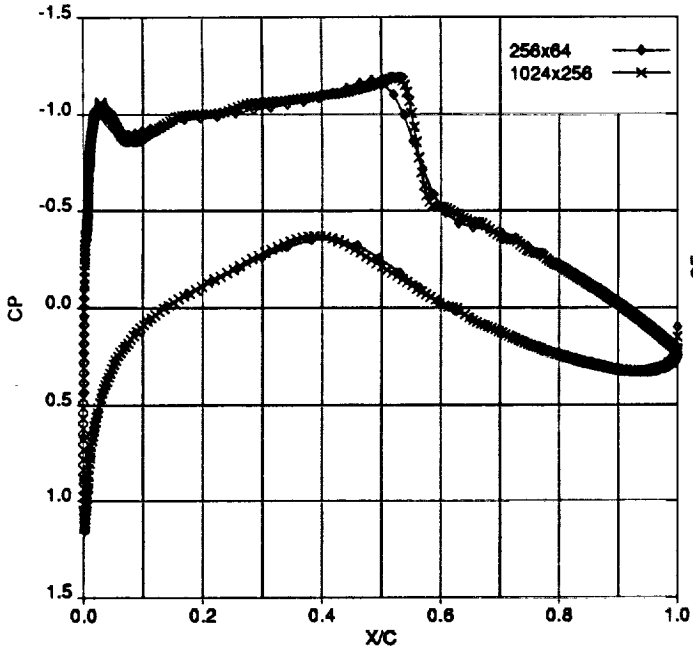

Figure 8: Pressure Distributions Computed on (256×64) and (1024×256) Grids for RAE 2822 Case 7.

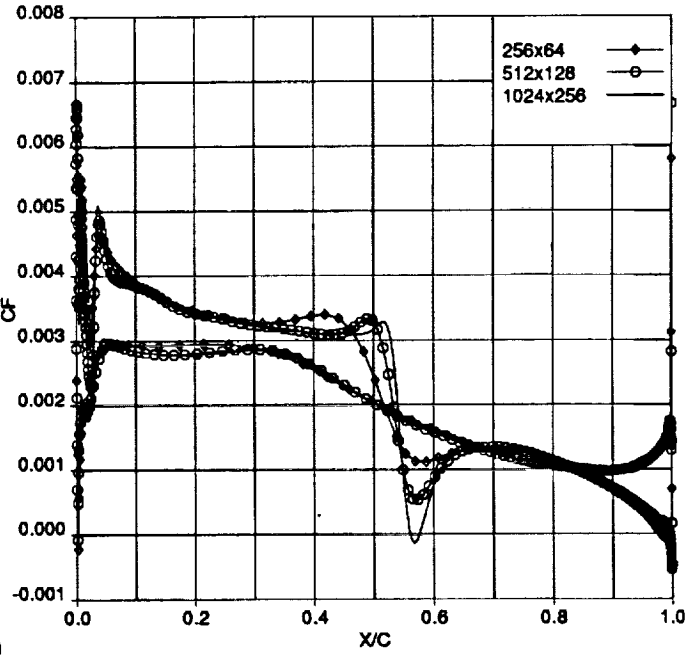

Figure 9: Skin Friction Computed on (256×64) through (1024×256) Grids for RAE 2822 Case 7.

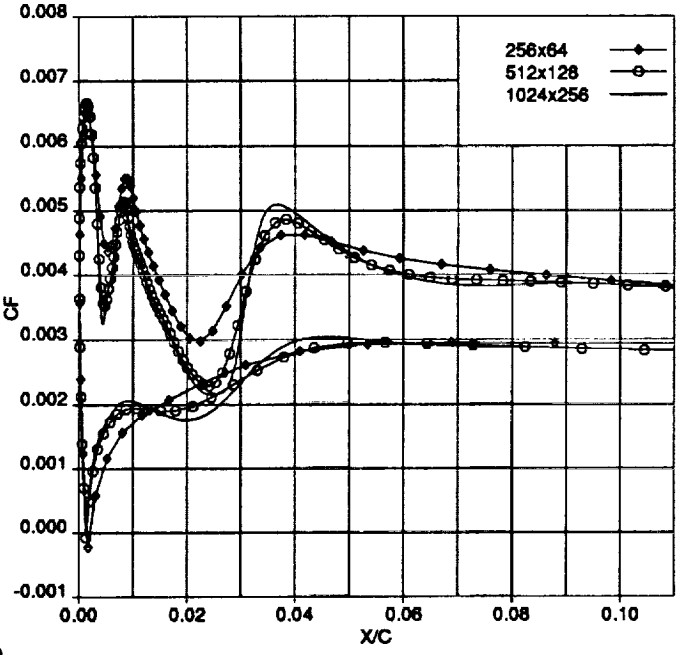

Figure 10: Skin Friction Computed on (256×64) through (1024×256) Grids for RAE 2822 Case 7 (Focus Near Leading Edge).

Navier-Stokes codes we have tried and for all turbulence models.

We realize that one must properly account for wind tunnel effects, especially for 2–D flows. However in the NACA 0012 test case it would require a Mach number reduction of more than 0.02 to produce a reasonable test/theory comparison. The large number of comparisons we have made between experimental data, ISES, and available 2–D Navier-Stokes codes suggest that there really is something wrong with the Navier-Stokes codes and/or the wind tunnel data which must be corrected.

2–D Grid Refinement Studies

As part of our program to find out if something is ailing the 2–D Navier-Stokes codes, we have taken advantage of the large memory afforded by our CRAY Y-MP to make exhaustive grid convergence studies. We have conducted such studies using the central-difference scheme of Martinelli and Jameson [2]. A grid refinement study for RAE 2822 case 7 is shown in figures (7) through (10). The flow conditions for this calculation were taken to be $M_\infty = 0.73$, $\alpha = 2.0°$ and $Re = 6.5 \times 10^6$ (based on chord). Transition was set at 3% of chord.

Trailing Edge Glitches

Glitches in the solution at the trailing edge are quite apparent. These glitches are characteristic of JT-NS codes for airfoils with a finite trailing-edge angle. The glitches do not go away with grid refinement. If anything, they tend to increase in amplitude. We have not found a satisfactory cure for these glitches but they can be ameliorated by turning off the fourth order artificial dissipation near the trailing edge.

Martinelli Compromise

On the 512 by 128 mesh (10), the transition from laminar to turbulent flow takes place over about 10 grid points. This spreading out of transition is caused by the "Martinelli Compromise" in the artificial dissipation, which has become common practice in JT-NS codes. The "Martinelli Compromise" is introduced to enhance convergence on grids with high-aspect ratio cells characteristic of a Navier-Stokes calculation [2]. Since JT codes depend on explicit time marching, the local time step they are permitted to use depends on how long it takes information to traverse the cell in the short direction. For a high aspect ratio cell this does not provide time for information to traverse the cell in the long direction. To ensure convergence, Martinelli dissipates the information traveling in the long direction by augmenting the artificial dissipation in this direction. The factor by which the artificial dissipation is augmented is proportional to the cell aspect ratio raised to the 2/3's power. Thus in the case of a 1000-to-1 aspect-ratio cell, the artificial dissipation in the long direction is multiplied by 100.

The "Martinelli Compromise" does serve to improve the speed and reliability of convergence, but as can be seen clearly at the transition point, the quality of the solution is indeed compromised. In some JT codes the ill effects of augmenting the artificial dissipation are diminished by reducing the 2/3's power to something smaller like 1/2 or even 0.3. The artificial dissipation in ARC2D [16] is essentially the same as that present in JT codes, except that no compromise is introduced. As a result, transition in ARC2D typically takes place over 3 points. On the other hand it has been our experience that ARC2D does not converge as reliably or as fast as JT codes.

Laminar Flow Convergence

In looking at figures (7) through (10) one notices that, as grid density is increased, the airfoil surface pressure distribution first begins to lock onto its grid converged values (with the exception of the immediate shock region), next the turbulent skin friction distribution locks in (but not at the shock), and finally (on unacceptably fine grids) the laminar skin friction distribution begins to lock in. We find it disturbing that a Navier-Stokes code would have so much trouble with laminar flow, particularly when compared to the resolution requirements for accurate solutions in boundary-layer codes.

For typical airfoils, the boundary layer is laminar for only a few percent of chord, and poorly resolved laminar regions often have little impact on the lift and drag calculations. However, we are also concerned with situations where laminar flow and transition prediction are important; hybrid laminar flow control and high-lift devices are two examples. For these flow fields, accurate prediction of laminar boundary layers on reasonable grids is crucial. The behavior at the shock (skin-friction reversal only on the 1024 by 256 grid) could also have an impact on the pressure drag.

SAD Laminar Flow Test Case

The poor performance of methods using scalar artificial dissipation (SAD) for high Reynolds number laminar flows can be demonstrated by considering flow over a flat plate at zero incidence. We present results for a laminar flat plate at a Reynolds number of $Re = 500,000$ and free stream Mach number of $M_\infty = 0.3$. More detailed results for this test case will be presented elsewhere.

Two numerical schemes are employed to solve this

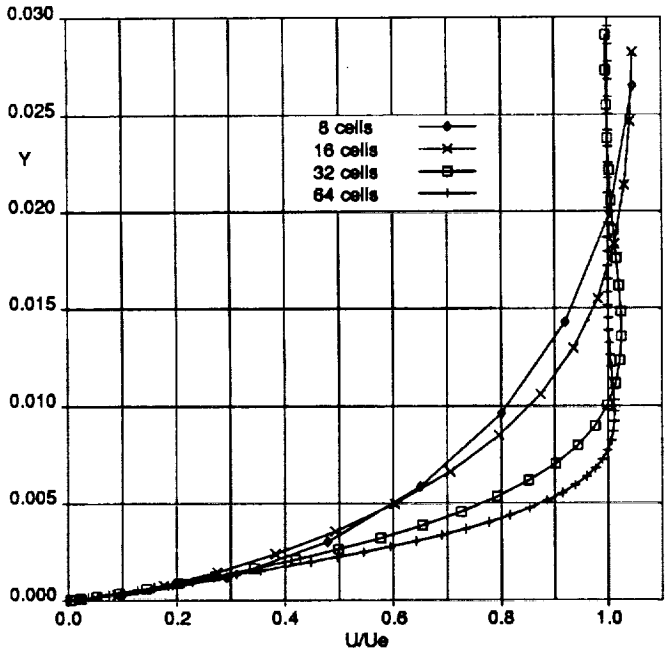

Figure 11: Grid Convergence of Velocity Profiles at $x = 1$ for Central Difference with Scalar Artificial Dissipation

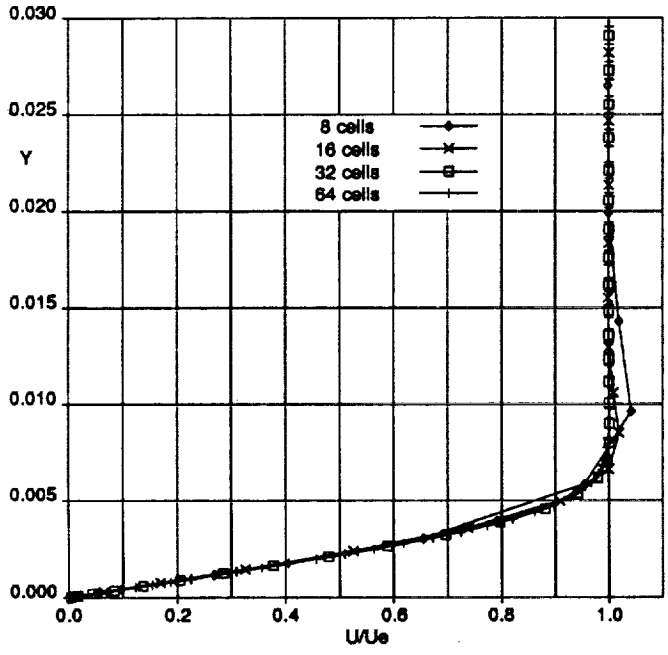

Figure 12: Grid Convergence of Velocity Profiles at $x = 1$ for Second-Order Upwind

Table 1: Central-Difference Boundary Layer Parameters at $x = 1$

grid	C_f (×1000)	δ^* (×1000)	θ (×1000)	$C_f Re_\theta$
16 × 8	1.683	6.240	3.514	2.956
32 × 16	1.693	5.343	2.741	2.321
64 × 32	1.124	2.977	1.158	0.651
128 × 64	0.965	2.564	1.009	0.487
Blasius	0.9390	2.434	0.9390	0.4409

Table 2: Upwind Boundary Layer Parameters at $x = 1$

grid	C_f (×1000)	δ^* (×1000)	θ (×1000)	$C_f Re_\theta$
16 × 8	1.006	2.435	1.096	0.5512
32 × 16	0.901	2.509	0.994	0.4481
64 × 32	0.919	2.465	0.956	0.4392
128 × 64	0.9318	2.450	0.9471	0.4413
Blasius	0.9390	2.434	0.9390	0.4409

flow. The first utilizes Jameson technology—central differencing with scalar artificial dissipation—to discretize the inviscid fluxes. The second scheme discretizes the inviscid fluxes using Roe's flux-difference splitting with second order upwind extrapolation of cell-centered states to cell faces [19]. Both schemes discretize the viscous fluxes using central differencing.

Figures (11) and (12) show velocity profiles at $x = 1$ unit downstream of the plate leading edge computed using the two numerical schemes. The profiles are computed on a sequence of four grids obtained by deleting every other grid line from the finest grid in the typical multigrid fashion. The finest grid contains 64 cells normal to the plate with the upper boundary at approximately three boundary layer thicknesses; the grid is parabolically stretched away from the plate. The grid is also parabolically stretched away from the leading edge in x with a grid spacing of approximately $\Delta x = 0.03$ at $x = 1$.

Figures (11) and (12) show much faster grid convergence for the profiles computed with the upwind scheme. The central-difference results are characterized by an overshoot in the velocity near the edge of the boundary layer and a significant thickening of the boundary layer. The two coarsest upwind profiles also show an overshoot, but that for the 16-cell grid is no worse than the result for the central difference scheme on the 64-cell

finest grid.

The disparity in accuracy between the central-difference and upwind solutions is further shown in Tables 1 and 2, where skin friction, displacement and momentum thicknesses are compared with the Blasius profile parameters at $x = 1$. Table 1 shows a quite rapid reduction in errors for the central-difference scheme with increased grid density (better than second order), but coarse grid errors are enormous compared to the upwind scheme results. For the 32-cell grid, the upwind solution contains approximately 18 cells within the boundary layer and gives 2% errors in the predicted parameters. This is consistent with our experience on resolution requirements for boundary layer solvers. In comparison, the central-difference results are still in error by 20% on this same grid.

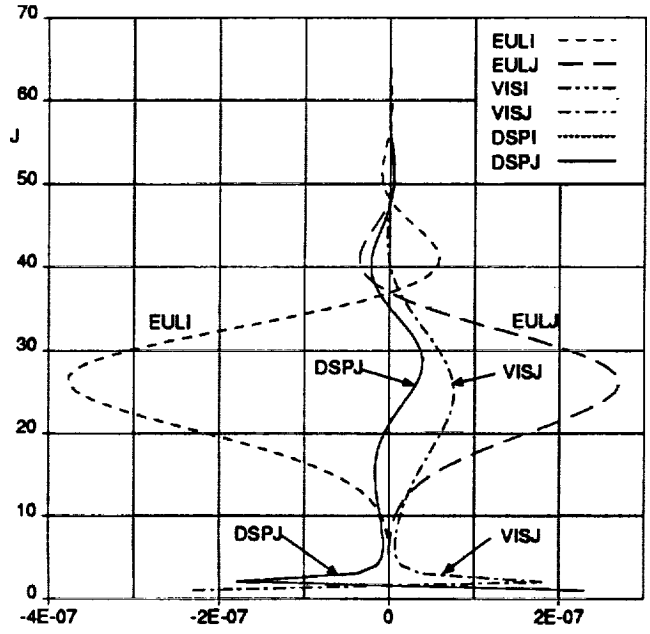

Figure 13: x-Momentum Equation Budget at $x = 1$ for Central Difference Scheme (64-cell grid)

We have identified the culprit for the relatively poor performance of the central-difference scheme; it is the scalar fourth-difference artificial dissipation in the normal direction; it is not related to the "Martinelli Compromise". Specifically, contamination results from excessive dissipation normal to the boundary layer in the x-momentum equation. This occurs because the artificial dissipation is scaled by the flux Jacobian spectral radius $|v| + c$, whereas a properly formulated matrix dissipation or upwind scheme (e.g. Roe's flux-splitting) scales the normal dissipation by $|v|$. It is easily shown that with the $|v| + c$ scaling, the normal artificial dissipation in the x-momentum equation is proportional to $(\Delta y/\delta)^3\sqrt{Re}/M$ based on edge conditions. Therefore, as the Reynolds number is increased, more grid resolution (i.e. more grid points across the boundary layer thickness δ) is required to achieve a given level of accu-

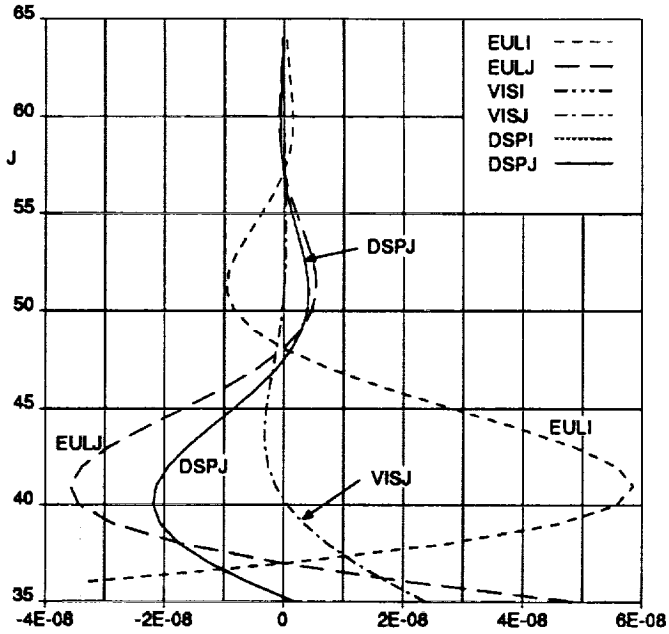

Figure 14: x-Momentum Equation Budget at $x = 1$ for Central Difference Scheme (64-cell grid) Blow-up of Boundary-Layer Edge

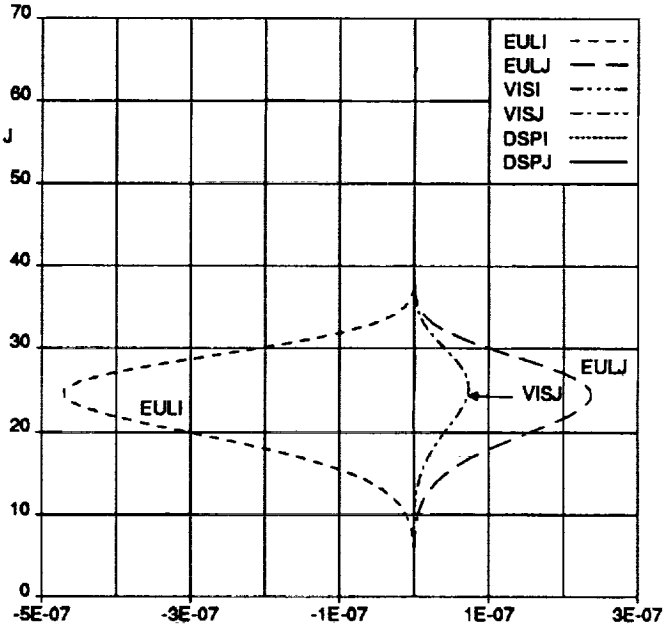

Figure 15: x-Momentum Equation Budget at $x = 1$ for Upwind Scheme (64-cell grid)

racy. This also explains why similar poor performance of scalar dissipation methods is not seen in low Reynolds number flows.

To illustrate the contamination, the budget for the x-momentum equation for the profile of cells at $x = 1$ is plotted in Figures (13), (14) and (15) for the central-difference and upwind schemes on the finest grid. In the figures, EULI, VISI and DSPI represent the difference in inviscid, viscous, and artificial dissipation fluxes, respectively, through the vertical faces of each cell (i.e. streamwise fluxes). EULJ, VISJ and DSPJ represent the analogous flux differences through horizontal faces (i.e. normal fluxes). For the upwind scheme, DSPI and DSPJ are taken as the difference of the split-fluxes and the face-averaged fluxes; hence, EULI and EULJ are consistently defined between the upwind and central-difference schemes.

Figures (13) and (14) reveal that the normal artificial dissipation (DSPJ) is large *everywhere* in the profile, even outside the boundary layer. Near the wall, the momentum balance is completely nonphysical with artificial dissipation (DSPJ) balancing viscous diffusion (VISJ). The budget for the upwind scheme is more physical; artificial dissipation is small everywhere, and the dominant terms are EULI, EULJ, and VISJ.

Some previous researchers have introduced ad hoc scaling reductions of the artificial dissipation through the boundary layer as an attempt to eliminate contamination. We have also applied some of these "fixes" with disappointing results, and know of no ad hoc scaling that will reduce the artificial dissipation across the entire profile to a point where the results are comparable to a properly formulated upwind scheme.

We wish to emphasize that these problems with high Reynolds number laminar flows are not inherent to central-difference schemes, but to central-difference schemes that use *scalar* artificial dissipation (CDSAD). This leads us to conclude that any scheme using scalar artificial dissipation or any scheme that is highly dissipative for low Mach number flows (e.g. van Leer's flux-splitting, see Ref. [5]), should be suspect for calculating laminar flows.

Our current research is directed towards improving the convergence rates of upwind schemes to steady-state. It is well known that reducing the spatial dissipation in a scheme usually results in slower convergence to steady-state.

2–D High-Lift Configurations

High-lift flow provides a significant challenge to CFD technology. For instance, the CFD code must have the ability to accurately predict the laminar boundary-layer profile ahead of the transition point so that a transition prediction method can be applied. The confluent boundary layer on the main element and the separated flows in the cove and on the flap must be modeled. There are free-shear layers in many parts of the flowfield where the spatial length scales of the flow characteristics are non-isotropic. The free-shear flows interact with the boundary layer on the flap to sometimes cause dramatic and unexpected flow behavior (e.g. Reynolds number reversal effects described in [8]). Simple boundary-layer approximations may not be adequate for such complex flows. Navier-Stokes methods seem to be the natural choice, but even here turbulence models remain a major issue.

We have written a code called A610 described in [17] that uses viscous/inviscid coupling to calculate flows around multi-element airfoil configurations. We will compare A610 with the Mavriplis unstructured grid NS code [18] for a Douglas 3 element configuration tested at LTPT. Comparisons between experiment, A610 and the Mavriplis code for 8, 20, and 23 degrees angle of attack are shown figures (16), (17), and (18). In order to run with A610, the coves on the lower surfaces of the leading edge slat and near the rear of the main element had to be smoothed. The effects of this smoothing are particularly noticeable in the A610 results at 8°. At all angles of attack A610 seems to predict C_p peaks that are a little too high. The overall test/theory comparisons seem to favor A610 at 20° and the Mavriplis code at 23°. At 8° A610 properly predicts separation for the trailing edge of the flap while the Mavriplis code does not. The inability to predict this flow separation seems to be a failing of the Chimera based Navier-Stokes codes as well.

Practical CFD assessment for High-Lift

Given these results there does not appear to be any strong reason for us to favor the Navier-Stokes code. All the more so since we know that being a NS-CDSAD code, the Mavriplis code is not able to properly calculate the laminar portions of the boundary layer and thus can not give us a transition prediction capability. The importance of transition, shown in figure (19), is computed using A610. When the Navier-Stokes codes come closer to achieving their theoretical potential, we will use them in earnest.

Also, while the preliminary capability in 2–D is being developed by many researchers, we badly need a 3–D code. In three dimensions, high-lift flow can be even more complex than in two dimensions. The edge vortices, gap flows, and embedded longitudinal vortices in the boundary layer all have strong effects on the overall performance of the high-lift system.

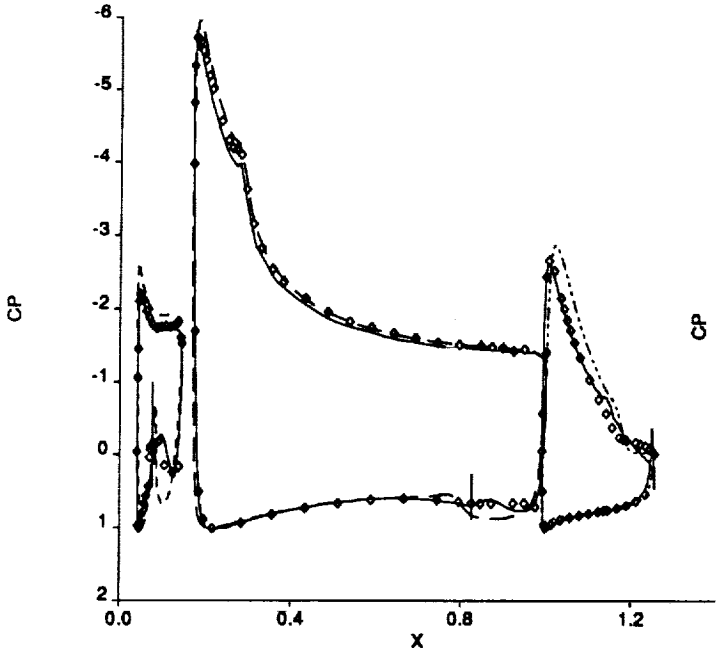

Figure 16: "High lift Olympics" 8° angle of attack. Experiment (Symbols) vs. Mavriplis (Lines) and A610 (Dashed-Lines)

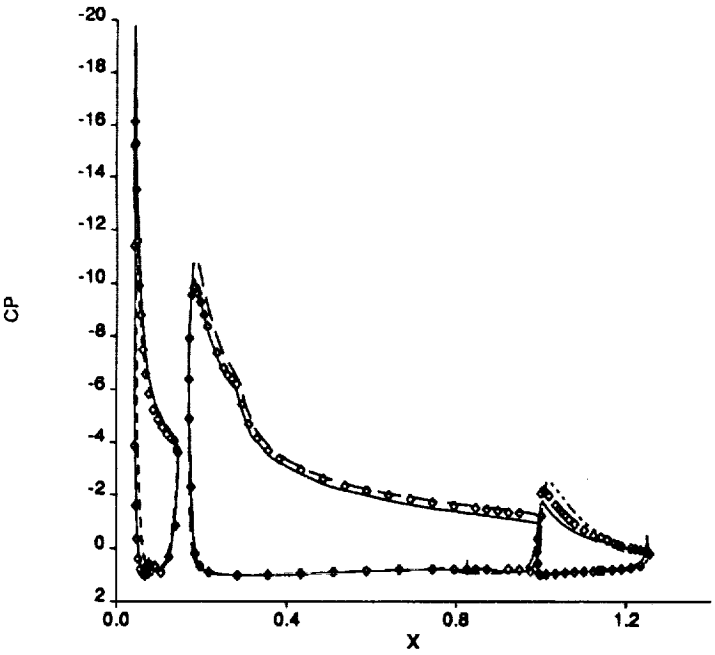

Figure 17: "High lift Olympics" 20° angle of attack. Experiment (Symbols) vs. Mavriplis (Lines) and A610 (Dashed-Lines)

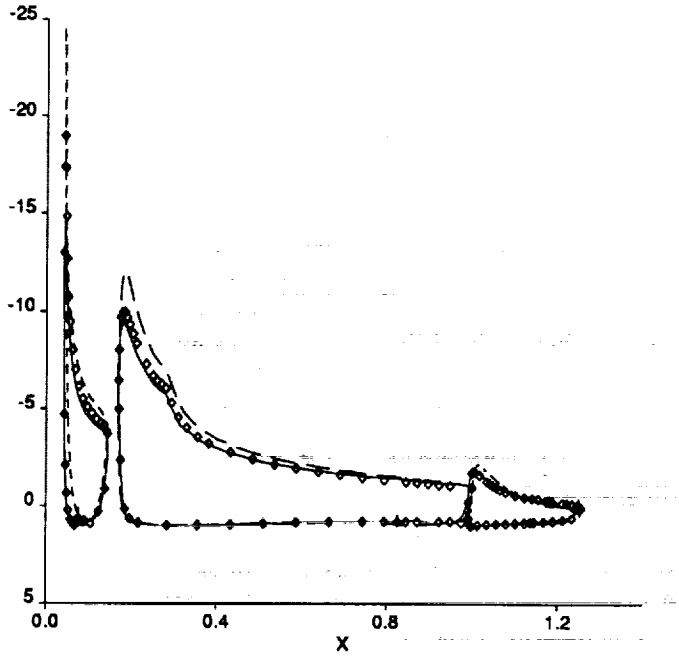

Figure 18: "High lift Olympics" 23° angle of attack. Experiment (Symbols) vs. Mavriplis (Lines) and A610 (Dashed-Lines)

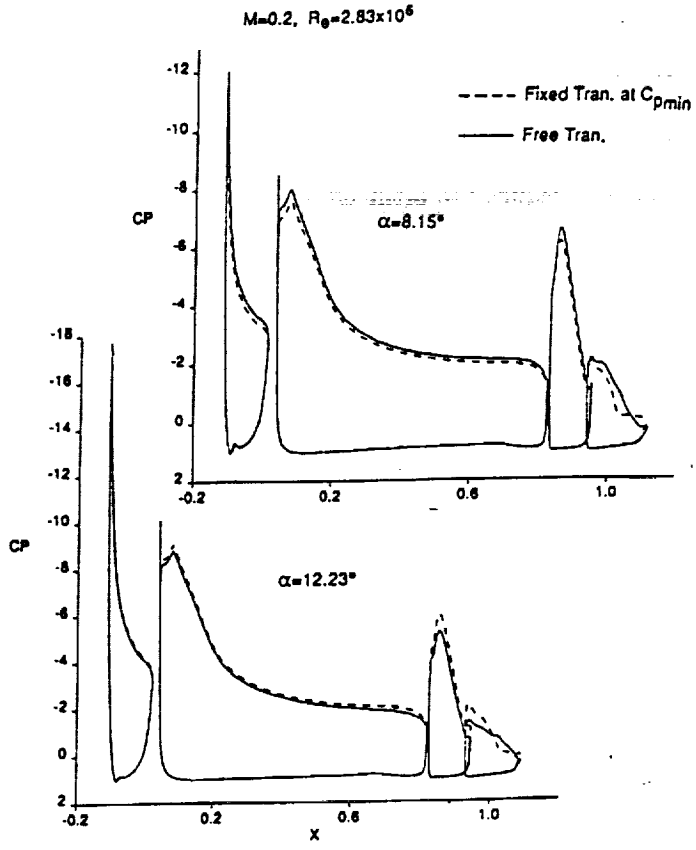

Figure 19: High lift, importance of transition

Nacelle-Flow Analysis

Nacelle analysis and design is an integral part of the airplane design process. In advanced aircraft, propulsion systems are closely coupled with the airframe, and proper engine installation is essential in order to improve the overall performance of the aircraft. Inviscid methods (panel and full-potential) have been very useful, but viscous effects are also of interest especially for off-design conditions on large twin-engine airplanes.

It is relatively easy to analyze an isolated flow-through nacelle using a code written to treat wings. We have adapted the TLNS3D Navier-Stokes code. The nacelle is treated as a ring wing, with periodic boundary conditions. To simulate a powered nacelle one can either specify inlet and exhaust boundary conditions, or use a center body with variable geometry to control the mass flux through in the engine. At cruise condition, the Navier-Stokes code provides accurate results, similar to that of wing or wing/body analysis. Problems are encountered in nacelle analysis with low-speed takeoff conditions, and with high-speed engine-out conditions.

At takeoff, the effective angle of attack for the nacelle is high. The flow is highly three-dimensional, and a laminar separation bubble may form at the nacelle highlight region. The marginal accuracy of the available Navier-Stokes codes in the laminar flow region was mentioned above. In the long run we must arrive at a reliable 3–D boundary-layer transition-prediction capability, as well as a plausible behavior in the transition region, before we can capture the laminar separation bubble. This bubble has dramatic effects on the overall flow field. Figure (20) compares the results of nacelle analysis, first treating the flow as fully turbulent (turbulence model active in the whole domain), and then assuming transition at 5% from the leading edge (turbulence model active only downstream of that line). The results are drastically different, and neither agree well with experiment. The flow pattern with transition at 5% is however similar to the experimental pattern.

At a high-speed, engine-out condition the large amount of spillage around the nacelle results in a strong shock on the exterior surface of the fan cowl, which may cause severe shock-induced separation. Present Navier-Stokes technology is capable of handling mild shock-induced separation. However, none of the turbulence models tested gives reliable solution for strong shock-induced separation.

In summary, attempts at nacelle analysis and engine-airframe integration by Navier-Stokes solutions raise the same issues as wing design. These are: gridding difficulties when other components are included; numerical accuracy particularly in the boundary layers; and turbulence-modeling accuracy particularly at shock interactions. In addition, because of lower Reynolds numbers and extreme velocity peaks at the lips, laminar regions may exist in the boundary layers and exert much control over the global flow field. In the long run we need a reliable and, as much as possible, automatic 3–D boundary-layer transition-prediction capability. For this, two key ingredients are—presumably—a stability analysis with sufficient robustness and generality to handle steep three-dimensional pressure gradients, and accurate velocity profiles directly out of the Navier-Stokes solver. Neither ingredient is at hand. The turbulence models also need improvement to handle moderate or massive separation, whether encountered at low-speed takeoff conditions or at high-speed, engine-out conditions.

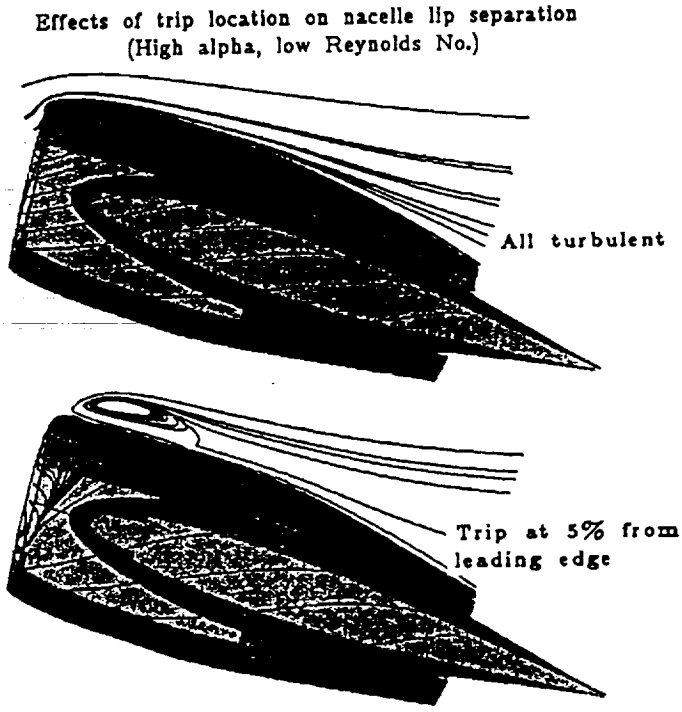

Figure 20: Nacelle with transition at 5% versus all turbulent flow

Conclusion

The 3-D Wing/Body calculations show that Navier-Stokes codes hold much promise. However, our test/theory comparisons in 2–D and for nacelles, as well as our detailed 2–D grid refinement studies, are sobering. It is apparent that much work remains to be done in numerics and physical modeling of transition and turbulence before we can say that we have an "Industrial-Strength" Navier-Stokes code in hand.

Acknowledgements

We wish to thank Steve Robinson (NASA Langley), Daryl Bonhaus (NASA Langely), Dimitri Mavriplis (NASA Langely), Frank Lynch (Douglas Aircraft Company), and Paul Meridith (Boeing) for helping us collect the data and computed results for the "High Lift Olympics" held at NASA Ames on May 2, 1991. Thanks to Wendy Wilkinson (Boeing) for rearranging the data and computed results so that they could (for the first time!) be plotted together and directly compared. Thanks also to Kevin Moschetti (Boeing) and Bill Newbold (Boeing) for providing ISES code results.

References

[1] Antony Jameson, "Successes and Challenges in Computational Aerodynamics," AIAA-87-1184, 1987.

[2] Luigi Martinelli, "Calculations of Viscous Flows with a Multigrid Method", Ph.D Thesis, Department of Mechanical and Aerospace Engineering, Princeton University, October, 1987.

[3] Swanson, R. C. and Turkel, E., "Artificial Dissipation and Central Difference Schemes for the Euler and Navier-Stokes Equations," AIAA-87-1107, 1987.

[4] Vatsa, V. N., and Wedan, B. W., "Development of an Efficient Multigrid Code for 3-D Navier-Stokes Equations," AIAA-89-1791, 1989

[5] Bram van Leer, James L. Thomas, Philip L. Roe, and Richard W. Newsome, "A Comparison of Numerical Flux Formulas for the Euler and Navier-Stokes Equations", AIAA-87-1104, 1987.

[6] Johnson, D. A., and Coakley, T. J., "Improvements to a Nonequilibrium Algebraic Turbulence Model," AIAA J., Vol. 28, No. 11, Nov., 1990

[7] Yu, N. J., Allmaras, S. R., and Moschetti, K. G., "Navier-Stokes Calculations for Attached and Separated Flows Using Different Turbulence Models," AIAA-91-1791, 1991

[8] Garner, P.L., Meridith, P.T., and Stoner, R.C., "Areas for Future CFD Development as Illustrated by Transport Aircraft Applications", AIAA-91-1527-CP, 1991.

[9] Yu, N. J., and Campbell, R. L., "Transonic Airfoil and Wing Design Using Navier-Stokes Codes," paper in preparation.

[10] Bengelink and Rubbert, "The Impact of CFD on the Airplane Design Process: Today and Tomorrow", iPAC International Pacific Air & Space Technology Conference and 29th Aircraft Symposium, Gifu, Japan, 1991.

[11] Bieterman, M. B., Bussoletti, J. E., Hilmes, C. L., Johnson, F. T., Melvin, R. G., Samant, S. S., and Young, D. P., "Solution Adaptive Local Rectangular Grid Refinement for Transonic Aerodynamic Flow Problems," Proceedings of the Eighth GAMM Conference on Numerical Methods in Fluid Mechanics, 1990, pages 22-31.

[12] Hafez, M. M., and Lovell, D., "Entropy and Vorticity Corrections for Transonic Flows," AIAA-83-1926, July 1983.

[13] Michael Giles and Mark Drela, "A Two-Dimensional Transonic Aerodynamic Design Method," AIAA-86-1793, 1986.

[14] Cook, P. H., McDonald, M. A., and Firmin, M. C. P., "Aerofoil RAE 2822 - Pressure Distributions, and Boundary Layer and Wake Measurements," AGARD-AR-138, pp. A6-1 through A6-77, May 1979.

[15] Thibert, J.J, Grandjacques M., and Ohman L. H., "NACA 0012 Airfoil," AGARD-AR-138, pages A1-1 through A1-36, May 1979.

[16] Thomas H. Pulliam, "Euler and Thin Layer Navier-Stokes Codes: ARC2D, ARC3D," Computational Fluid Dynamics Workshop held at the University of Tennessee Space Institute, Tullahoma, Tennessee, March 12-16, 1984, pages 15.1 through 15.85.

[17] Kusonose, K., Wigton, L., and Meredith, P., "A Rapidly Converging Viscous/Inviscid Coupling Code for Multi-Element Airfoil Configurations," AIAA-91-0177, January 1991.

[18] Dimitri Mavriplis, "Turbulent Flow Calculations Using Unstructured and Adaptive Meshes," ICASE Report No. 90-61, September 1990.

[19] Roe, P. L., "Approximate Riemann Solvers, Parametric Vectors, and Difference Schemes," Journal of Computational Physics, Vol. 43, 1981, pp. 357-372.